HHS Public Access

Author manuscript

Acta Neuropathol. Author manuscript; available in PMC 2021 October 01.

Published in final edited form as:

Acta Neuropathol. 2021 April ; 141(4): 547–564. doi:10.1007/s00401-021-02288-1.

Heterogeneity in α-synuclein fibril activity correlates to disease phenotypes in Lewy body dementia

Arpine Sokratian[1], **Julia Ziaee**[1], **Kaela Kelly**[1], **Allison Chang**[1], **Nicole Bryant**[1], **Shijie Wang**[1], **Enquan Xu**[1], **Joshua Y. Li**[1], **Shih-Hsiu Wang**[2,3], **John Ervin**[2,3], **Sandip M. Swain**[4], **Rodger A. Liddle**[4], **Andrew B. West**[1,2]

[1]Department of Pharmacology and Cancer Biology, Duke Center for Neurodegeneration Research, Duke University, 3 Genome Court, Durham, NC 27710, USA

[2]Department of Neurology, Duke Center for Neurodegeneration Research, Duke University, Durham, NC, USA

[3]Department of Pathology, Duke Center for Neurodegeneration Research, Duke University, Durham, NC, USA

[4]Department of Medicine, Duke Center for Neurodegeneration Research, Duke University, Durham, NC, USA

Abstract

α-Synuclein aggregation underlies pathological changes in Lewy body dementia. Recent studies highlight structural variabilities associated with α-synuclein aggregates in patient populations. Here, we develop a quantitative real-time quaking-induced conversion (qRT-QuIC) assay to measure permissive α-synuclein fibril-templating activity in tissues and cerebrospinal fluid (CSF). The assay is anchored through reference panels of stabilized ultra-short fibril particles. In humanized α-synuclein transgenic mice, qRT-QuIC identifies differential levels of fibril activity across the brain months before the deposition of phosphorylated α-synuclein in susceptible neurons. α-Synuclein fibril activity in cortical brain extracts from dementia with Lewy bodies (DLB) correlates with activity in matched ventricular CSF. Elevated α-synuclein fibril activity in CSF corresponds to reduced survival in DLB. α-Synuclein fibril particles amplified from cases with high fibril activity show superior templating in the formation of new inclusions in neurons relative to the same number of fibril particles amplified from DLB cases with low fibril activity. Our results highlight a previously unknown broad heterogeneity of fibril-templating activities in DLB that may contribute to disease phenotypes. We predict that quantitative assessments of fibril activities in CSF that correlate to fibril activities in brain tissue will help stratify patient populations as well as measure therapeutic responses to facilitate the development of α-synuclein-targeted therapeutics.

Andrew B. West, Andrew.West@Duke.edu.

Supplementary Information The online version contains supplementary material available at https://doi.org/10.1007/s00401-021-02288-1.

Keywords

SNCA; Prion; Biomarker; Aggregation; Neurodegeneration; Parkinson's disease

Introduction

The aggregation of α-synuclein typifies pathology in synucleinopathies that include Parkinson's disease (PD), dementia with Lewy bodies (DLB), and multiple system atrophy (MSA). α-Synuclein monomers can assemble into a number of different disease-associated conformers [3]. These conformers may include long and rigid rods, ribbons, and spheroid-like assemblies [2, 10]. Exogenously produced α-synuclein fibrils, so-called pre-formed fibrils, are rapidly internalized by different cells and can corrupt the endogenous complement of α-synuclein into cytotoxic aggregates in a prion-like fashion [1, 31]. Assays designed to recognize the presence of templating fibril conformers in tissues and biofluids include protein misfolding cyclic amplification (PMCA) and the related real-time quaking-induced conversion (RT-QuIC) approaches. Both methodologies have demonstrated robust efficacy in detecting very low levels of α-synuclein aggregates harbored in CSF samples from Lewy body diseases and MSA that distinguish cases from controls [6, 12, 41, 44, 45, 47].

Several recent studies have identified specific differences in fibril compositions found in different synucleinopathies. With the PMCA approach, Shahnawaz et al. demonstrated differential levels of amyloid-binding fluorescence from MSA versus PD, with control tissues and fluids unable to promote similar fibril-templating activities [45]. However, Strohaeker et al. concluded that fibrils amplified from PD did not exhibit distinctive structural properties from MSA [47]. Rather, a structural diversity in fibrils amplified from five different PD brain extracts was identified [29, 40]. Several studies agree that DLB-associated α-synuclein fibrils fail to propagate efficiently compared to MSA fibrils [29, 37, 40, 48]. Fibrils amplified from either DLB or PD were three orders of magnitude less potent in templating new inclusions in neurons compared to MSA-derived fibrils [37, 48]. However, given the results of Strohaeker et al., variabilities might exist within groups of DLB patients that might confound broader interpretations from a few subjects.

DLB-amplified fibrils have been difficult to analyze on an ultra-structure level because they might bear non-descriptive straight-rod conformations in electron microscopy analysis that apparently lack twists or other demarcating morphologies [44, 49]. On a functional level, in measurements of templating activities in the formation of new fibrils, PMCA and RT-QuIC approaches have been primarily utilized in a qualitative manner with respect to PD and DLB brain extracts and CSF. Given the broad clinical and pathological heterogeneity associated with DLB [11, 35], and the aforementioned functional heterogeneity [47, 49], we predict that assays with higher sensitivity and specificity for resolving functional fibril-templating characteristics and activities might shed light on the relationship between DLB endophenotypes and the prion-like characteristics of DLB-associated α-synuclein fibril strains.

In developing a quantitative approach for the measurement of α-synuclein fibril-templating activity in DLB brain extracts and CSF, we observed unexpectedly high stability of extremely short human α-synuclein fibril preparations. The robust stability associated with these particles facilitated their integration into standard curves to measure permissive α-synuclein fibril-templating activity in DLB brain extracts and CSF. In our case series, a very high level of fibril activity correlates to an early death after a diagnosis of dementia. Permissive α-synuclein fibril-templating activity was not predicted through other pathological measures of α-synuclein, phosphorylated tau, blood contamination of CSF, or other concomitant pathologies. These observations demonstrate the potential power of qRT-QuIC in identifying endophenotypes that might correspond to prion-like fibril activities in Lewy body dementia.

Materials and methods

Animal and human approvals

All study protocols were approved by the local Institutional Review Board and the Institutional Animal Care and Use Committee. Mice were housed under environmentally controlled standard conditions with a 12-h light/dark cycle and free access to food and water. Strains used include WT-hPAC-α-synuclein mice (PAC-Tg (*SNCA*^{WT}); *Snca*$^{-/-}$), JAX stock #010710), knockout-α-synuclein mice (*Snca*$^{-/-}$, JAX stock #016123) and C57BL/6J (WT (nTg) control mice (JAX stock #000664). Females and males were equally distributed in groups throughout the study. Mice were randomly assigned to each group. Tissues were processed in coded samples, and investigators blinded to group identity, with assignment to groups after final data curation.

Brain and cerebrospinal fluid samples

Human post-mortem brain tissues (middle frontal cortex, Brodmann area 46) and matched CSF samples (drawn from both lateral ventricles) were obtained from the Bryan Brain Bank and Biorepository at Duke University. Selected demographics and clinical information are provided in Table 1. All DLB cases were clinically diagnosed and pathologically confirmed as neocortical-type DLB according to the McKeith criteria [32, 33]. Lewy body density in the neocortex was quantified based on McKeith criteria, where score 1 was assigned to tissue sections (middle frontal cortex Brodmann area 46) with < 1 Lewy body/100 × field (0.22 × 0.22 μM), score 2 with 1–4 Lewy bodies, score 3 with 4–10 Lewy bodies, and score 4 greater than 10 Lewy bodies/designated field [33]. AD pathology was evaluated according to the 2012 NIA-AA guidelines [22]. Fresh frozen tissues were Dounce-homogenized in at 50 × weight/volume in 1% Triton-X-100 (IBI Scientific, Cat# IB07100) phosphate-buffered saline (Corning, Cat# 21-040-CM) and further processed with probe-tip sonication to homogeneity for following qRT-QuIC analysis. For immunoblotting, fresh frozen tissues were subjected to homogenization in 1% Triton-X-100 supplemented with protease inhibitors (Sigma, Cat# 4693132001). Lysates and CSF samples were centrifuged at 20,000×g for 20 min at 4 °C, and supernatants aliquoted into Lo-bind (Eppendorf, Cat# 925000090) microfuge tubes for further experiments.

ssFibril generation and characterization

Bacterial expression plasmids encoding mouse and human α-synuclein were de novo synthesized (GenScript) with optimized codons for expression in *E. coli* in the inducible pRK172 backbone and BL21 (DE3-RIL) CodonPlus cells (Agilent, Cat# 230245-41). Cell pellets were lysed in 10 mM Tris–HCl, pH 7.6, 0.75 M NaCl, 1 mM EDTA, 1 mM PMSF (ACROS, Cat# AC215740050), and sonicated at 70% power (Fisherbrand, Model 500 Dismembrator) for 1 min. Tubes were placed in boiling water for 15 min. Pellets were discarded and supernatants dialyzed into 10 mM Tris–HCl, pH 7.6, 50 mM NaCl, 1 mM EDTA, and 1 mM PMSF. Supernatants were processed through a HiPrep Q HP 16/10 Column, 1 × 20 mL (GE Healthcare) on an Akta Pure protein purification system (GE Healthcare, Cat# 29018182) with a running buffer composed of 10 mM Tris–HCl pH 7.6, 25 mM NaCl, and eluted with a linear gradient application of high-salt buffer (10 mM Tris–HCl, pH 7.6, 1 M NaCl). Samples containing single bands for α-synuclein (Coomassie staining) were combined, dialyzed, and concentrated. Endotoxins were removed (GenScript, Cat# L00338) to below 0.1 endotoxin unit/mg of protein as determined by LAL chromogenic endotoxin quantification (GenScript, Cat# L00350C). Final concentration of protein (monomer) was determined by both BCA assay (Pierce, Cat# 23227) and Nanodrop analysis (A_{280}). Mouse or human spontaneous α-synuclein fibrils were prepared by incubation of 7 mg/mL α-synuclein monomer in phosphate-buffered saline in protein lo-binding tubes for 4 days at 37 °C with constant agitation at 800 rpm in a thermomixer (Eppendorf, Thermomixer Compact 5350 Mixer). Fibrils were centrifuged at 20,000×g for 20 min at room temperature and washed pellets subjected to sonication with active liquid cooling maintenance of temperature set to 10 °C (Q-Sonica, Model Q700). Sonicated fibril preparations were mixed at a ratio of ~ 1:1000 w/v with monomer at 37 °C with constant agitation for a second round of amplification (Fig. 1a), with subsequent washed pellets sonicated as indicated. CSF-derived fibrils were prepared by incubation of 2 mg/mL α-synuclein monomer in phosphate-buffered saline for 4 days at 37 °C with constant agitation. Fibrils were centrifuged at 20,000×g for 20 min at room temperature, and washed pellets were subjected to sonication with active liquid cooling maintenance with a temperature set to 10 °C (Q-Sonica Q700). All preparations were measured by dynamic light scattering on a Titan DynaPro (Wyatt Technology) at 25 °C with the Dyna V6.3.4 software package. For recombinant and CSF-derived ssFibrils, dynamic light scattering analysis was first subjected to estimate the homogeneity level of each preparation and evaluate size distribution (supplemented with EM data). Samples with polydispersity index < 0.5 were considered as homogeneous and pertinent for measurement. A dynamic light scattering coil model was applied for size estimation of ssFibrils and monomer in the Dyna V6.3.4 software environment. Molecular weight of ssFibrils was calculated based on known CryoEM fibril dimensions with measured dynamic light scattering and electron-microscopy consensus size distributions.

Transmission electron microscopy

0.1 mg/mL samples were applied to glow-discharged 300 mesh, carbon-only, copper grids (LADD, Cat# 10873-25) and negatively stained with 0.5% uranyl acetate (Polysciences, Cat# 21447-25). Grids were imaged with a FEI Tecnai F20 electron microscope (Eindhoven)

operated at 200 kV with nominal magnification at 65,000 × and a defocus range of – 1.0 to – 1.27 μM. Images were collected on a Gatan Ultrascan 4000 CCD camera.

qRT-QuIC analysis

All reactions were performed in ultra-low binding 384-well plates (Corning, Cat# 4588) with clear bottoms and sealed with foil (BioRad, Cat# MSF1001). Reactions in phosphate-buffered saline (as indicated), supplemented with 10 μM thioflavin-T (Sigma, Cat# T3516-25g), 20 μM α-synuclein monomer, spiked in with the known concentration of ssFibrils into the same matrix as experimental samples under evaluation (e.g., brain lysates, CSF, saline, etc.). Prior to incubation, each well was supplemented with a 2.3 mM diameter zirconia silica bead to accelerate the reaction (Bio-Spec Products, Cat# 11079125Z). Reaction fluorescence was monitored on FLUOstar Omega (BMG) plate reader for the indicated time with 60 s of shaking at 700 rpm followed by 60 s of resting. Thioflavin-T signal was recorded every 30 min at 448–10 nM excitation and 482–10 nM emission.

Determination of fibril-forming units (FFUs)

Time-dependent thioflavin-T fluorescence values collected from qRT-QuIC fibrillization curves, background subtracted, were exported in CSV files and processed with custom software searches that analyze cycle time (C_T) and corresponding increased rate of change of fluorescence in each replicate. Iterative code loops evaluate possible threshold cut-offs that return the threshold value yielding the highest linear correlation coefficient in standard curves of known ssFibrils. Coding paths are provided via GitHub (https://github.com/west-lab/FibrilOptimization/blob/master/FibrilPaperCode_main.py) for use in python-compatible platforms. Known number of ssFibrils ends (tenfold diluted, from 10^9 (Lg9) to 10 (Lg1) added to qRT-QuIC reactions were used to recreate standard log-linear regression curves of FFUs for determination of unknown FFUs in experimental groups. Log-linear regression standard curves are considered successful based on $r > 0.9$, with experimentally determined C_T(h) values compared to known concentrations of ssFibrils that estimate permissive templating activity in solution.

Mouse primary neuron cell culture

Post-natal (P0) mice were placed on ice for 5-min, brains were removed, and hippocampi dissected into Hibernate E medium (BrainBits, Cat# HE). Tissue was triturated into papain solution (Worthington Biochemical, Cat# LS003119) in HBSS buffer (Sigma, Cat# H9394-1L) supplemented with 10 mM HEPES pH 7.4, 100 mM sodium pyruvate, and 1% penicillin/streptomycin (Thermofisher, Cat# 15140122). Neurons were plated with Neurobasal media (Thermofisher, Cat# 21103049) supplemented with 1 × B27 (Thermofisher, Cat# 17504044), 5 mM GlutaMAX (Thermofisher, Cat# 35050061), and 10% fetal bovine serum (ATL-BIO, Cat# S11150H, Q-39042) onto poly-D-lysine (Sigma, Cat# P0899) coated surfaces at a density of 1×10^5 cells/cM^2. Two hours after plating, medium was exchanged with Neurobasal media supplemented with GlutaMAX and B27 supplement. At day-in-vitro (DIV) 7, ssFibrils were added to each well of neurons to a final concentration 0.62 nM. After 10 days of incubation, neurons were fixed and subsequently used for immunostaining.

Immunohistochemistry and immunofluorescence

For paraffin-embedded human formalin-fixed brain tissue, sections were de-paraffinized in xylene followed by ethanol rinses. Sections were treated with 1.875% H_2O_2 in methanol for 8 min, formic acid treatment (Sigma, Cat# F0507) for 30 s, washed, and incubated in 5% w/v nonfat dry milk in 50 mM Tris–HCl, pH 7.6, for 20 min. Antibodies included Syn-1 (BD Transduction Laboratories, Cat# 610787), Tau-AT8 (Pierce, Cat# MN1020), and rabbit anti-mouse HRP (Agilent Technologies, Cat# S080983-2), with Dako DAB solution (Agilent Technologies, Cat# K346811-2). Some sections were counterstained with Hematoxylin+ reagent (Fisher, Cat# 22-220-100).

Fixed 40 μM mouse brain sections were incubated in an antigen recovery solution of 10 mM sodium citrate, pH 6.0, supplemented with 0.05% tween-20, at 37 °C for 1 h with gentle rocking. Sections were quenched for 30 min at room temperature with 0.3% H_2O_2 in methanol and rinsed with Tris-buffered saline (TBS, pH 7.4). Sections were incubated in blocking buffer (5% goat-serum with 0.3% Triton X-100 in TBS) for 1 h at room temperature and primary antibodies pS129-α-synuclein (20 ng/mL, EP1536Y, Abcam, Cat# ab51253) were applied for 48 h at 4 °C. Secondary antibodies (AffiniPure Donkey Anti-Rabbit IgG, Jackson Immunologic, Cat# 711-065-152) conjugated to biotin were used and sections treated with the ABC kit (Vector Labs, Cat# PK-6100) followed by development with Impact 3,3'-diaminobenzidine (DAB) reagent (Vector Labs, Cat# SK-4105). Sections were dehydrated progressively in ethanol, Histo-Clear (National Diagnostics, Cat# HS2001GLL), and then mounted to coverslips with Permount reagent (Fisher, Cat# SP15100). Slides were analyzed on an Olympus BX61 wide field microscope.

Primary neurons were treated with 2% paraformaldehyde (Electron microscopy, Cat# 15714S) in PBS for 15 min, subsequently incubated for 30 min at room temperature in 3% goat-serum (Equitech-Bio, Cat# SG32-05) with 0.1% saponin (Sigma, Cat# 47036) in PBS. Primary antibodies were applied in the 1% goat-serum, 0.02% saponin buffer with pS129-α-synuclein (20 ng/mL, EP1536Y, Abcam) and Tau (0.5 μg/mL, Tau-5, Invitrogen, Cat# AHB0042), overnight at 4 °C. Neurons were rinsed and then a solution of secondary antibodies, Goat anti-rabbit AlexaFluor 555, 4 μg/mL, Abcam, Cat# ab150078, Goat anti-mouse AlexaFluor 647, 4 μg/mL, Abcam, Cat# ab150115, with DAPI stain (1 μg/mL, ThermoFisher, Cat# 62248) for 3 h at room temperature. Images were obtained and analyzed by investigators blinded to sample identity on a Keyence BZ-X810 microscope using the manufacturer's software.

Immunoblotting

Mice brain sections were collected and dissected following transcranial perfusion with cold PBS. Mice brain compartments and post-mortem brain samples were homogenized in 50 × vol/weight in 1% triton X-100 supplemented saline and complete protease and phosphatase inhibitors (Roche Cat# 11697498001 and 4906845001) followed by probe-tip sonication. Homogenates were centrifuged at 10,000×g for 10 min at 4 °C. Supernatants were analyzed using BCA assay (Pierce) to determine total protein concentration and were then further diluted 1:1 with 2 × Laemmli sample buffer supplemented with 10% DTT (RPI, Cat# D11000-25.0). Lysates were analyzed on 4–20% gradient mini-PROTEAN TGX stain-free

gels (Biorad, Cat# 4568085). Stain-free gels were activated for 45 s through UV transilluminator (Chemidoc MP Imaging System, BioRad) and total protein load was analyzed by visualization by UV excitation. Activated TGX stain-free gels were transferred to 0.2 μM pore-size nitrocellulose membrane (Biorad, Cat# 1620112), followed by capturing transferred to membrane a total protein load through UV transilluminator (Chemidoc MP Imaging System, BioRad). Transferred membranes were then immunoblotted with primary antibodies for human (syn-211, Abcam, Cat# ab80627) or for both human and mouse (syn80-96, Biolegend, Cat# 848302) α-synuclein detection, and secondary goat anti-mouse HRP (Jackson Immunologic, Cat# 115-035-003) antibodies. Crescendo ECL reagent (Millipore Sigma, Cat# WBLUR0500) was used to develop chemiluminescent signals. All signals were captured digitally using a Chemidoc MP Imaging System (BioRad). Quantifications were performed using Image Lab 6.0.1 software (BioRad).

Single-molecule detection (SiMOA) and chemiluminescence-enhanced ELISA assays

SiMOA pTau-181 kit (Quanterix, Cat# 103377) was used according to manufacturer's instructions for the analysis of human CSF on the SR-X platform. The LEGEND MAX™ human α-synuclein ELISA Kit (Biolegend, Cat# 844101) was used to determine total α-synuclein concentrations according to manufacturer's instructions. Signals were recorded on a ClarioStar plate reader (BMG).

Statistics

Statistical analyses (see Figure legends) were conducted using Graphpad Prism 8.0 software.

Results

High stability of short-stumpy α-synuclein fibril reference panels for RT-QuIC assays

Protein fibrils have been described as rigid structures generally prone to breakage and disaggregation in practice [8, 9, 25, 36, 46, 52]. In particular, α-synuclein fibril assemblies are unstable [39]. We and others have demonstrated that ultra-sonication of human WT-α-synuclein filaments can rapidly shred particles to terminal lengths without disaggregation [1, 7]. The ultra-sonicated α-synuclein fibrils bear a characteristic short stumpy fibril (ssFibril) cylindrical appearance in transmission electron microscopy analysis, amenable to dynamic light-scattering characterization. We introduce the term ssFibrils to describe homogenous preparations of ultra-sonicated α-synuclein fibrils that share these biophysical characteristics (illustrated in Fig. 1a, b). Through an iterative process resembling PMCA that includes sedimentation, shredding, re-amplification, and shredding again, other α-synuclein conformers that might include oligomers or disordered large aggregates are selectively depleted from the ssFibril preparations (Fig. 1a).

We set out to systematically probe the resiliency of ssFibrils under physiological conditions. Since human- and mouse-derived α-synuclein fibrils are commonly used in Lewy body disease-related research (human and mouse α-synuclein sequence differing at key residues for aggregation [21]), we chose to examine ssFibrils with either human or mouse sequence. Our investigations revealed that both mouse and human ssFibrils at physiological pH and ionic strength do not fragment, disaggregate, or aggregate into larger structures over 12 days

of observation at either 4 °C or room temperature (~ 25 °C) (Fig. 1c; Supplemental Fig. 1). High homogeneity of fibril preparations over time was further confirmed by polydispersity analysis (Supplemental Fig. 1). At physiological temperature (i.e., 37 °C), human ssFibrils show minor signs of aggregation, while mouse ssFibril self-aggregation is substantial (Supplemental Fig. 1a, b). Amyloid conformations of both human and mouse ssFibrils were unperturbed over time as determined by thioflavin-T binding (Supplemental Fig. 1). ssFibrils were also extraordinarily resilient to freeze–thaw fracturing, with only ~ 20% conversion after ten consecutive freeze–thaw cycles.

In contrast to ssFibrils, full-length α-synuclein fibrils rapidly devolved into smaller conformers and monomer admixtures after a few freeze–thaw cycles, consistent with the highly unstable nature of long α-synuclein fibrils noted by others (Fig. 1d, e; [39]). These results are consistent with ssFibrils bearing a higher tensile strength and resiliency compared to longer fibrils, a property previously found for other very short fibrils [4, 19, 38]. Our results suggest that α-synuclein ssFibrils maintain the amyloid conformation and relative size, amenable to light-scattering analysis, apparently resisting further aggregation under different conditions and timeframes. In contrast, the long parental fibril structures that share the same amyloid configuration are highly unstable.

The ultra-structure of human α-synuclein fibrils from Li et al. and Guerrero-Firreira et al. both identified a 1.97 nM height/length that includes ten monomer subunits (Fig. 1f; [20, 30]). We imputed this averaged value into the ssFibril preparations characterized with dynamic light scattering and electron microscopy to determine an average molecular weight estimate (average length of ssFibrils—30 nM, where every 1.97 nM stack consists of ten monomeric α-synuclein units) and particle concentration for ssFibrils in solution. Based on past studies of fibril polymerization characteristics and the assumption that the ssFibril is the smallest template-permissive fibril unit, two possible template permissive ends are assigned to each fibril particle [5]. With these assumptions, we establish the concentration of estimated maximum number of fibril ends in solution. We refer to this measurement as fibril-forming units (FFUs) throughout.

Development of quantitative RT-QuIC for human α-synuclein fibrils

We evaluated reference pools of human ssFibrils using RT-QuIC assays across nine orders of magnitude differences in spiked-in ssFibril concentration (Fig. 1g; Supplemental Fig. 2). Thioflavin-T binding was measured at different time points for each ssFibril dilution and analyzed with custom software designed to optimize threshold values for highest performance across the dilutions (Supplemental Fig. 2). Cycle threshold values (i.e., C_T) indicate the time interval for an individual reaction to reach the calculated thioflavin-T fluorescence threshold. The quantitative RT-QuIC (qRT-QuIC) approach allows detection of fibril ends across these dilutions, with an apparent lower limit of detection corresponding to ~ 10 ssFibrils in the reaction in a 384-well format (~ 2 zeptomol of monomer equivalent, Fig. 1h). In comparison, a recent study under different RT-QuIC assay conditions showed a detection limit for a qRT-QuIC assay of ~ 0.5 femtomol of monomer equivalent with linearity across five orders of magnitude [42].

Within this assay sensitivity, we examined specificity in the detection of ssFibrils with different sequences of α-synuclein, for example, in cross-species reactivity in the detection of mouse α-synuclein ssFibrils. The qRT-QuIC assay was wholly intolerant to cross-seeding between human and mouse α-synuclein ssFibrils, as well as to mismatched monomer α-synuclein templating substrate in the assay (Supplemental Fig. 2). Specificity reached the level of single-residue alterations in the α-synuclein protein sequence since a single variant (p.K80M) substitution in the human α-synuclein sequence rendered the assay incapable of detecting different concentrations of fibrils over nine orders of magnitude of ssFibrils spiked into the reactions (Supplemental Fig. 2). These results demonstrate that the performance of qRT-QuIC is extremely constrained in sequence but highly dynamic over a wide range of fibril concentrations in measuring like sequences of α-synuclein fibrils.

Early fibril activity in the brains of human α-synuclein-expressing mice

To assess sensitivity of the qRT-QuIC assay within the complexity of brain tissue extracts, we derived lysates from regionally dissected brains of mice with knockout of endogenous mouse α-synuclein and the expression of human WT α-synuclein via the human α-synuclein promoter (PAC-Tg($SACA^{WT}$); $Snca^{-/-}$), or an α-synuclein knockout with no α-synuclein expression. Whole-brain lysate analysis showed the transgenic mice express total α-synuclein at ~ fourfold over endogenous mouse α-synuclein (e.g., ~ 10 ng/mg of brain tissue in endogenous α-synuclein versus ~ 40 ng/mg of brain tissue with PAC-driven α-synuclein expression), with nominal increases in α-synuclein protein in different brain regions from 1 month to 1 year of age (Supplemental Fig. 3). With the transgenic over-expression, the mice show age-dependent cytoplasmic depositions of pS129-α-synuclein across the brain by 1 year of age, whereas no pS129-α-synuclein signal could be detected in knockout mice as expected (Fig. 2a; and consistent with past reports [13, 16]).

Discordant from pS129-α-synuclein pathology, qRT-QuIC identified an early high abundance of fibril-forming activity (calculated FFUs) from triton-X-100 extracts of fresh tissues from regionally dissected brain regions in recently weaned mice (e.g., 1-month-old). In these assays, ssFibril reference libraries were spiked into comparable triton-X-100 solubilized reference brain lysates derived from α-synuclein knockout mice to approximate buffer and matrix conditions across assay wells. High FFUs found in the striatum and other tissues in the humanized α-synuclein mice did not reduce with aging (Fig. 2b, c). Rather, the cerebellum presented with low FFUs at 1 month and later ~ 100-fold higher levels of FFUs in 1-year-old mice (Fig. 2c). In contrast, total α-synuclein expression increased very slightly in the cerebellum from ~ 10 ng/mg of tissue at 1 month to ~ 14 ng/mg of tissue at 1 year (Supplemental Fig. 3). Midbrain extracts, harboring the substantia nigra and other brain regions, had the most variable concentrations of FFUs measured per mg of brain tissue (Fig. 2c), without apparent changes in total α-synuclein expression with age. Thus, the expression of total α-synuclein protein did not predict fibril-forming activities found in qRT-QuIC assays.

qRT-QuIC analysis of DLB brain tissue uncouples fibril activity from α-synuclein expression

Given our results from mouse brain extracts with overexpression of human WT-α-synuclein (Fig. 2; [27]), we asked whether abundant fibril activity could also be detected in brain extracts processed in the same way from neocortical-type DLB cortical tissue (middle frontal cortex Brodmann area 46) and controls. Case and control clinical and demographic information is presented in Table 1. We acquired post-mortem brain samples with neocortical-type DLB and mixed Alzheimer's disease (AD) pathology. As expected, many of the DLB-affected brains were also positive for neocortical tau pathology (AT8, Braak stages IV–VI) and amyloid pathology (Fig. 3a). All control brain tissues were evaluated for pathology and negative for α-synuclein, tau, and amyloid in the neocortex. Protein lysates were generated from each brain sample with the same lysis buffer used in the humanized α-synuclein mice and measured for α-synuclein protein concentration. We observed no difference in α-synuclein concentration (ng of α-synuclein per mg of brain tissue) between DLB and control samples in our extracts (Supplemental Fig. 4).

In comparing DLB and control tissues, median FFUs per mg of brain tissue were increased approximately 100,000-fold in DLB lysates versus control brains, leading to significant but imperfect group separation of cases versus controls (Fig. 3b, c, AUC = 0.88, $p < 0.0001$). α-Synuclein protein concentration in the extracts did not correlate with measured FFUs ($r = -0.09$, $p = 0.6$, Fig. 3d). Nearly half (6 of 14) of the control group demonstrated low FFUs levels (< 10 FFUs/ng of α-synuclein). The remaining eight control brains (similarly negative for Lewy bodies, tangles, and amyloid plaques) had significant FFUs that overlapped in abundance with some DLB cases, ranging from 100 to 1,000,000 FFUs/mg of brain tissue. Evaluation of the DLB panel of lysates stratified against Lewy body density, post-mortem interval, and Braak staging for concomitant tau tangle pathology (Supplemental Fig. 4) or high AD pathology (Fig. 3e) revealed no correlations or differences between groups. Therefore, neither co-occurring tau tangles, abundancy of Lewy body inclusions, nor amyloid plaques, appeared to predict FFU measurements in the DLB cohort.

qRT-QuIC analysis of CSF from DLB patients implicates high fibril activity in reduced survival

α-Synuclein fibril-templating activity has been observed in lumbar CSF from PD, DLB, and more rarely in neurologically healthy control subjects [14, 18, 23]. Using matched ventricular CSF fluids to compare with the brain tissue samples analyzed herein (Table 1), we observed a robust separation of DLB cases from controls, with ROC AUCs of 0.94 for FFUs normalized to CSF volume (Fig. 4a, b). These results are consistent with the aforementioned past studies using lumbar CSF. In the application of the qRT-QuIC assay, 27 of 31 DLB CSF samples demonstrated > 200 FFUs/mL of CSF, with 13 of 31 DLB samples demonstrating extremely high activity in > 1,000,000 FFUs/mL of CSF (Fig. 3a). α-Synuclein concentration in CSF did not predict FFU concentration well, with a weak negative correlation noted ($r = -0.34$, $p < 0.005$, Fig. 4c). α-Synuclein concentration in CSF was similar between DLB and controls (Supplemental Fig. 5). Separation by tau or AD-pathological diagnosis (e.g., high versus low AD pathology) did not reveal group differences in measured CSF FFUs (Fig. 4d; Supplemental Fig. 5). These results suggest neither

concomitant tau nor amyloid pathology, or pathological estimations of Lewy body density in the neocortex, influences measures of α-synuclein fibril activity in CSF. Measures of hemoglobin levels in the CSF, a marker of hemolysis and blood contamination inherent to ventricular CSF, failed to reveal a specific influence of blood contamination with FFUs, either positive or negative, in correlation analysis ($r = 0.07$, $p > 0.5$, Supplemental Fig. 6). p181-Tau levels in the CSF were also uncorrelated with FFUs ($r = 0.18$, $p = 0.23$, Supplemental Fig. 6). However, a correlation was noted between p181-tau levels and α-synuclein levels in CSF, similar to previous published reports with lumbar CSF ($r = 0.6$, $p < 0.0001$, Supplemental Fig. 6; [50]).

A moderate correlation between FFUs found in cortical brain tissue extracts and CSF FFUs was identified, irrespective of whether FFUs are normalized by weight/volume or to ng of α-synuclein in the sample ($r = 0.55$, $p < 0.001$, or $r = 0.45$, $p < 0.002$, Fig. 5a, b). In DLB cases, we noticed the highest FFU concentrations corresponded to DLB cases with death soon after a diagnosis of DLB. Overall correlation between FFUs and survival after a diagnosis of DLB was moderate ($r = -0.40$, $p = 0.027$, Fig. 5c). CSF fibril activity was highest in those individuals who died early within 5 years of diagnosis (median values ~ 250-fold-elevated for fibril activity in CSF, $p = 0.0015$, receiver operating curve (ROC) area-under the curve (AUC) = 0.82, Fig. 5e). Higher FFU concentrations in the whole case and control cohort trended towards negative correlations with mini-mental state examination (MMSE) scores for those subjects where scores were available ($r = -0.40$ for CSF and $r = -0.58$ for brain tissues, $p = 0.06$ and $p = 0.005$, respectively, see Supplemental Fig. 7), although correlation within cases was not significant ($r = 0.20$ for CSF and $r = -0.37$ for brain tissues, $p = 0.56$ and $p = 0.28$, respectively, see Supplemental Fig. 7). Biological sex (Fig. 5f) did not appear to significantly affect FFU measures in CSF or brain tissue (two-way ANOVA, Sidak's multiple comparison corrected, $p = 0.84$ for CSF and 0.40 for brain tissue). In the brain tissue of DLB cases, measured FFUs were similar between males and females in this cohort (Fig. 5f, median FFUs 5.3 for females and 6.6 for males, $p = 0.061$, Mann–Whitney U test).

With the assumption that fibril-forming activity can be attributed primarily to α-synuclein multimeric conformers in the lysates (e.g., fibrils), stoichiometric calculations of fibril-forming ends suggest a major fraction of the soluble compartment (i.e., triton X-100 solubilized) of α-synuclein in human brain tissue may be composed of very short structures permissive to α-synuclein fibrillation (Fig. 5g). In CSF, the fraction of α-synuclein that might be aggregated is much lower, and essentially non-existent in controls without Lewy body disease. An alternative hypothesis could involve other factors present in the lysates that may synergize with monomeric or non-fibrillized α-synuclein in driving high-apparent FFU measures in qRT-QuIC assays.

Diverse α-synuclein strain properties in ssFibrils amplified from DLB CSF

Recent studies have demonstrated distinctive α-synuclein strain properties in fibrils amplified from MSA to those from PD and DLB tissues [28, 44, 45]. DLB α-synuclein strains have been described as refractory to differential structural analysis and may have lower potency compared to MSA strains in seeding characteristics [44]. Through

consecutive rounds of amplification, we noticed that all DLB strains prepared as ssFibrils (~ 30 nM short-rod fibrils measured by light-scattering) lagged behind in Thioflavin-T half-maximal fluorescent curves in qRT-QuIC curves as compared to equivalent concentrations of ssFibrils generated through spontaneous fibrillation, suggesting different thioflavin-T binding characteristics or possible differential downstream growth kinetics, or both (Fig. 6a, b). We could not detect any differences between the different strains in dynamic light scattering analysis (Fig. 6c).

To determine the relative templating activity of the ssFibrils to corrupt the endogenous complement of human α-synuclein in neurons, known concentrations of ssFibrils were added to primary neurons expressing human α-synuclein (knockout of mouse α-synuclein). pS129-α-synuclein-positive inclusions that matured in the cytoplasm were measured 10 days later (Fig. 6d–g; Supplemental Fig. 8). Application of the same number of α-synuclein ssFibril particles to primary hippocampal neurons revealed that ssFibrils purified from a DLB CSF sample with low-yield FFUs per ng of α-synuclein in the CSF (< 10,000 FFUs/ng of α-synuclein) poorly templated new inclusions. In contrast, ssFibrils purified from CSF samples with high-yield FFUs per ng of α-synuclein (> 1,000,000 FFUs/ng of α-synuclein) templated new inclusions in neurons with higher apparent efficiency, approximating that of spontaneously generated ssFibrils. In each experiment, the same numbers of ssFibril particles were added to the neurons, qualified with light-scattering analysis (Fig. 6c). In this culture system, none of the fibril treatments resulted in a significant loss of NeuN or DAPI-positive cells in the wells over the timeframe that was evaluated (Supplemental Fig. 8). These results suggest qRT-QuIC measures may be predictive of templating activities associated with different fibril strains in neurons. Further, spontaneously generated and purified α-synuclein fibrils produced with very high concentrations of α-synuclein under optimal conditions (e.g., ssFibrils studied here) may align closer in strain properties with the most aggressive strains amplified from DLB cases.

Discussion

Our conclusions center on four novel observations. First, we found that human α-synuclein fibrils shredded to very small lengths have exceptional stability under physiological conditions, with preserved amyloid properties and fibril-templating activity noted in real-time quaking-induced conversion assays (RT-QuIC). The production of reference panels of ultra-short α-synuclein fibril particles facilitated the optimization of RT-QuIC assays to produce outstanding ($r = 0.97$) log-linear relationships with threshold thioflavin-T fluorescence across nine orders of magnitude of human α-synuclein fibril concentration. Second, using newly minted quantitative RT-QuIC assays, we found evidence of very early fibril-templating activity shortly after weaning in the brains of mice over-expressing WT human α-synuclein, months before the apparent deposition of phosphorylated cytoplasmic α-synuclein in susceptible neurons. Third, in the analysis of fibril burden in CSF procured from DLB cases, we found that high fibril loads were more common in the cases with an early death after a diagnosis of DLB. Fourth, in comparative analysis of the fibril particles from selected DLB cases, the high fibril activity amplified particles from an early-death DLB case had higher templating activity in neurons than the low fibril-templating activity

amplified particles. Together, these results support a model where α-synuclein fibril heterogeneity in disease may affect outcomes in Lewy body dementia (Fig. 7).

The qRT-QuIC assay variant used here was optimized for log-linearity across a range of known ssFibril concentrations. The assay is anchored with standard curves generated by pools of stable short and stumpy ssFibrils derived from long filaments that can be spiked into a variety of matrices, including brain extracts and CSF. The ssFibrils are not structurally different species than their parental filaments according to thioflavin-T affinity, but become highly protected from further breakage or self-aggregation under physiological conditions. Unlike substantial stability observed for human ssFibrils, mouse ssFibril equivalents appeared less likely to retain structural properties at physiological temperatures over time. We predict that the differential stability of fibrils and other types of aggregates imparted by different amino acid sequence substitutions in α-synuclein could have a profound effect on stability that may confound some experimental endpoints in different experiments.

During the course of our experiments, a variation of qRT-QuIC was described that demonstrated positive assay performance in accurately measuring serial dilutions of recombinant α-synuclein seeds with or without added control CSF [42]. The authors concluded that CSF does not inhibit the RT-QuIC reaction through linear regression calculations of the lag phase for each dilution [42]. Our results agree, and we significantly extend the performance of this approach using custom software that calculates threshold values (C_T) optimized for linear responses of known fibril-forming units (FFUs) within 384-well micro-reactions. The assay and accompanying software theoretically accommodate a wide variety of diverse matrices that include different lysates, detergents, and buffer combinations, so long as the reference particles are spiked into the same matrix as the experimental samples. Future assay optimization may improve variability in repeat reactions between wells and improve the steepness of the slope across different fibril concentrations to enhance sensitivity. While past studies utilizing small fibrils in disease modeling studies typically report the amount of α-synuclein (i.e., in monomer equivalents) added into different experimental models, there are no functional titers reported from standardized approaches in most studies, making cross-study comparisons using different pools of fibrils in different laboratories difficult to understand. We propose qRT-QuIC as a valuable tool ready to rapidly assign functional titers to α-synuclein particles measured from either clinical samples or in disease models, with titers reported with respect to spontaneously generated ssFibrils as described.

Increases in WT α-synuclein expression through allelic multiplication in humans cause widespread fibrillary α-synuclein pathology throughout much of the brain [17, 24]. The pathology in the neocortex in α-synuclein triplication carriers is often reminiscent of DLB-cortical-type pathology [15, 26, 51]. We applied qRT-QuIC to probe brain tissues from a transgenic mouse model that expresses WT α-synuclein fourfold over endogenous mouse α-synuclein. Interestingly, the mouse transgenic tissue at ~ 10–40 ng of α-synuclein per mg of brain tissue in different brain regions was similar to the concentration ranges of α-synuclein found in the human neocortical brain tissue pieces we analyzed, where most DLB cases had 5–40 ng of α-synuclein per mg of tissue. The mouse model allowed analysis of brain tissue months before the apparent deposition of cytoplasmic phosphorylated α-synuclein, with our

collection taking place shortly after weaning in juvenile mice. We observed striking fibril activity in soluble fractions from the brains of juvenile mice, apparently in brain regions without noticeable accumulations of α-synuclein. Fibril activity does not wane through life in the mouse model but varies several orders of magnitude in abundance in different brain regions. We hypothesize that very short fibrillary α-synuclein species, representing just a small fraction of the total pool of α-synuclein in neurons, drives our fibril activity measurements. We further predict that these very rare fibril species, generated very early on, may accumulate into insoluble larger aggregates over time. We predict that these age-related cytoplasmic depositions of phosphorylated α-synuclein would not be measured efficiently in our qRT-QuIC assay owing to the insoluble nature of the aggregates and possible inaccessibility of the fibril ends. Introduction of aggressive denaturants, acids, and strong sonic shearing protocols into insoluble fractions may render the triton X-100 insoluble aggregates more amenable to characterization with our qRT-QuIC assay.

Soluble pools of high molecular weight α-synuclein in neocortical DLB tissue have been previously hypothesized to drive early dysfunction in disease [43], potentially consistent with hypotheses formulated around soluble pools of amyloid as determinants of severity of neurodegeneration in AD [34]. In patients diagnosed clinically and pathologically with DLB, we noted a broad heterogeneity of fibril activity in different samples. Unexpectedly, fibril activities were identified in most neurologically normal controls, otherwise negative pathologically for Lewy body diseases and Alzheimer's disease. Further evaluation of brain tissues from a much wider range of ages and different brain regions may provide further insights into whether fibril activity may be physiological or a pre-aggregate aberration associated purely with disease. We speculate that the latter scenario is more likely, given the extreme rarity of the species in the control tissues as determined with our quantitative assays compared to the vast abundance of the total pool of α-synuclein protein.

In the controls analyzed here, fibril activity was not observed in ventricular CSF, even though fibril activity (albeit at a low level) was detected in matched brain tissue samples. We hypothesize that co-occurring neurodegeneration in disease is a required part of fibril release into CSF. Or, a disease-associated process may actively export FFU-associated cofactors into CSF in the context of disease without the necessity of overt cell loss. A better understanding of the major pathways that facilitate fibril export from cells in ongoing disease would facilitate interpretation of our results. Neither blood contamination nor co-occurring AD pathology appears to influence observed α-synuclein fibril activity in the CSF samples. This is consistent with the high-sequence constrained performance of α-synuclein qRT-QuIC, where even a single amino acid substitution can render the assay insensitive to seeding. We predict that longitudinal studies measuring fibril activities through the course of disease in larger cohorts of lumbar CSF samples with qRT-QuIC assays will provide much more sensitivity to resolve specific endophenotypes that may underlie survival probability in disease.

The specific conformers of α-synuclein that drive apparent fibril activity in DLB cases in this study were not identified and may be considerably heterogeneous in nature, requiring further study to better understand structure-function relationships. It is conceivable that strains more labile to breakage early on in amplification (before threshold fluorescence)

could inflate apparent FFU measures in the rapid de novo generation of new fibrils ends during initial phases of templating and thioflavin-T binding. Further, if a strain cannot bind thioflavin-T, our assay would not record the presence of that strain. However, if the starting conformers in the experimental lysates are small oligomers or fibrils, according to our modeling, they would represent a very small percentage of the total concentration of α-synuclein in the extracts. The rarity of these species may obviate traditional orthogonal means of detection (e.g., detection with conformer-specific antibodies or mass spectrometry methods) that may considerably lack the required sensitivity.

One recent study demonstrated that DLB strains amplified from a PMCA technique displayed modest or no seeding potential in different models [49]. Our results are overall in agreement that some DLB-fibril strains present with very low templating activity in comparison to spontaneous fibril preparations of α-synuclein. However, our results also suggest that other DLB cases from high-burden fibril carriers do match with potencies observed in optimized spontaneous fibril preparations of α-synuclein. The broad heterogeneity identified here presents challenges to the interpretation of past studies drawing conclusions from the evaluation of only a few samples from Lewy body dementia cases. Conceivably, patient-specific fibril models could be constructed to determine the differences with respect to neurodegeneration, spread across the brain, and associated neuroinflammatory processes with different strains. The approaches and results described here may facilitate the stratification of different cases and controls in experimental studies. Further, we would predict that qRT-QuIC might be utilized in measuring efficacies of experimental therapeutics designed to reduce burdens of pathological α-synuclein in the brain, with both quantitative metrics at baseline measures and in drug responses.

Supplementary Material

Refer to Web version on PubMed Central for supplementary material.

Acknowledgements

These studies have been supported by the National Institutes of Health grants P50 NS108675 and R01 NS064934. The authors acknowledge the generous contributions made by study participants and their families to further research into the causes of DLB and to help find treatments. The authors are indebted to the Duke Kathleen Price Bryan Brain Bank and Biorepository, a component of the Joseph and Kathleen Bryan Alzheimer's Disease Research Center at Duke University. The authors thank Valentina Krendelchtchikova for her technical assistance, and Sara Miller and Ricardo Vancini for assistance with electron microscopy carried out with the Duke Electron Microscopy Service.

References

1. Abdelmotilib H, Maltbie T, Delic V, Liu Z, Hu X, Fraser KB et al. (2017) α-Synuclein fibril-induced inclusion spread in rats and mice correlates with dopaminergic neurodegeneration. Neurobiol Dis 105:84–98. 10.1016/j.nbd.2017.05.014 [PubMed: 28576704]
2. Bousset L, Pieri L, Ruiz-Arlandis G, Gath J, Jensen PH, Habenstein B et al. (2013) Structural and functional characterization of two alpha-synuclein strains. Nat Commun 4:2575. 10.1038/ncomms3575 [PubMed: 24108358]
3. Brás IC, Dominguez-Meijide A, Gerhardt E, Koss D, Lázaro DF, Santos PI et al. (2020) Synucleinopathies: where we are and where we need to go. J Neurochem 153:433–454. 10.1111/jnc.14965 [PubMed: 31957016]

4. Buehler MJ (2006) Nature designs tough collagen: explaining the nanostructure of collagen fibrils. Proc Natl Acad Sci USA 103:12285–12290. 10.1073/pnas.0603216103 [PubMed: 16895989]
5. Buell AK (2019) The growth of amyloid fibrils: rates and mechanisms. Biochem J 476:2677–2703. 10.1042/bcj20160868 [PubMed: 31654060]
6. Candelise N, Schmitz M, Llorens F, Villar-Piqué A, Cramm M, Thom T et al. (2019) Seeding variability of different alpha synuclein strains in synucleinopathies. Ann Neurol 85:691–703. 10.1002/ana.25446 [PubMed: 30805957]
7. Chatani E, Lee YH, Yagi H, Yoshimura Y, Naiki H, Goto Y (2009) Ultrasonication-dependent production and breakdown lead to minimum-sized amyloid fibrils. Proc Natl Acad Sci USA 106:11119–11124. 10.1073/pnas.0901422106 [PubMed: 19564620]
8. Chen GF, Xu TH, Yan Y, Zhou YR, Jiang Y, Melcher K et al. (2017) Amyloid beta: structure, biology and structure-based therapeutic development. Acta Pharmacol Sin 38:1205–1235. 10.1038/aps.2017.28 [PubMed: 28713158]
9. Chiti F, Dobson CM (2006) Protein misfolding, functional amyloid, and human disease. Annu Rev Biochem 75:333–366. 10.1146/annurev.biochem.75.101304.123901 [PubMed: 16756495]
10. Conway KA, Lee SJ, Rochet JC, Ding TT, Williamson RE, Lansbury PT Jr (2000) Acceleration of oligomerization, not fibrillization, is a shared property of both alpha-synuclein mutations linked to early-onset Parkinson's disease: implications for pathogenesis and therapy. Proc Natl Acad Sci USA 97:571–576. 10.1073/pnas.97.2.571 [PubMed: 10639120]
11. Coughlin DG, Hurtig HI, Irwin DJ (2020) Pathological influences on clinical heterogeneity in Lewy body diseases. Mov Disord 35:5–19. 10.1002/mds.27867 [PubMed: 31660655]
12. De Luca CMG, Elia AE, Portaleone SM, Cazzaniga FA, Rossi M, Bistaffa E et al. (2019) Efficient RT-QuIC seeding activity for α-synuclein in olfactory mucosa samples of patients with Parkinson's disease and multiple system atrophy. Transl Neurodegener 8:24. 10.1186/s40035-019-0164-x [PubMed: 31406572]
13. Delic V, Chandra S, Abdelmotilib H, Maltbie T, Wang S, Kem D et al. (2018) Sensitivity and specificity of phospho-Ser129 α-synuclein monoclonal antibodies. J Comp Neurol 526:1978–1990. 10.1002/cne.24468 [PubMed: 29888794]
14. Fairfoul G, McGuire LI, Pal S, Ironside JW, Neumann J, Christie S et al. (2016) Alpha-synuclein RT-QuIC in the CSF of patients with alpha-synucleinopathies. Ann Clin Transl Neurol 3:812–818. 10.1002/acn3.338 [PubMed: 27752516]
15. Farrer M, Kachergus J, Forno L, Lincoln S, Wang DS, Hulihan M et al. (2004) Comparison of kindreds with parkinsonism and alpha-synuclein genomic multiplications. Ann Neurol 55:174–179. 10.1002/ana.10846 [PubMed: 14755720]
16. Gispert S, Del Turco D, Garrett L, Chen A, Bernard DJ, Hamm-Clement J et al. (2003) Transgenic mice expressing mutant A53T human alpha-synuclein show neuronal dysfunction in the absence of aggregate formation. Mol Cell Neurosci 24:419–429. 10.1016/s1044-7431(03)00198-2 [PubMed: 14572463]
17. Goedert M, Spillantini MG, Del Tredici K, Braak H (2013) 100 years of Lewy pathology. Nat Rev Neurol 9:13–24. 10.1038/nrneurol.2012.242 [PubMed: 23183883]
18. Groveman BR, Orrù CD, Hughson AG, Raymond LD, Zanusso G, Ghetti B et al. (2018) Rapid and ultra-sensitive quantitation of disease-associated α-synuclein seeds in brain and cerebrospinal fluid by αSyn RT-QuIC. Acta Neuropathol Commun 6:7. 10.1186/s40478-018-0508-2 [PubMed: 29422107]
19. Guérin G, Wang H, Manners I, Winnik MA (2008) Fragmentation of fiberlike structures: sonication studies of cylindrical block copolymer micelles and behavioral comparisons to biological fibrils. J Am Chem Soc 130:14763–14771. 10.1021/ja805262v [PubMed: 18847270]
20. Guerrero-Ferreira R, Taylor NM, Mona D, Ringler P, Lauer ME, Riek R et al. (2018) Cryo-EM structure of alpha-synuclein fibrils. Elife. 10.7554/eLife.36402
21. Hong L, Ko HW, Gwag BJ, Joe E, Lee S, Kim YT et al. (1998) The cDNA cloning and ontogeny of mouse alpha-synuclein. NeuroReport 9:1239–1243. 10.1097/00001756-199804200-00051 [PubMed: 9601701]
22. Hyman BT, Phelps CH, Beach TG, Bigio EH, Cairns NJ, Carrillo MC et al. (2012) National institute on aging-Alzheimer's association guidelines for the neuropathologic assessment of

Alzheimer's disease. Alzheimers Dement 8:1–13. 10.1016/j.jalz.2011.10.007 [PubMed: 22265587]

23. Kang UJ, Boehme AK, Fairfoul G, Shahnawaz M, Ma TC, Hutten SJ et al. (2019) Comparative study of cerebrospinal fluid α-synuclein seeding aggregation assays for diagnosis of Parkinson's disease. Mov Disord 34:536–544. 10.1002/mds.27646 [PubMed: 30840785]
24. Kim WS, Kågedal K, Halliday GM (2014) Alpha-synuclein biology in Lewy body diseases. Alzheimers Res Ther 6:73. 10.1186/s13195-014-0073-2 [PubMed: 25580161]
25. Knowles TP, Waudby CA, Devlin GL, Cohen SI, Aguzzi A, Vendruscolo M et al. (2009) An analytical solution to the kinetics of breakable filament assembly. Science 326:1533–1537. 10.1126/science.1178250 [PubMed: 20007899]
26. Konno T, Ross OA, Puschmann A, Dickson DW, Wszolek ZK (2016) Autosomal dominant Parkinson's disease caused by SNCA duplications. Parkinsonism Relat Disord 22(Suppl 1):S1–6. 10.1016/j.parkreldis.2015.09.007 [PubMed: 26350119]
27. Kuo YM, Li Z, Jiao Y, Gaborit N, Pani AK, Orrison BM et al. (2010) Extensive enteric nervous system abnormalities in mice transgenic for artificial chromosomes containing Parkinson disease-associated alpha-synuclein gene mutations precede central nervous system changes. Hum Mol Genet 19:1633–1650. 10.1093/hmg/ddq038 [PubMed: 20106867]
28. Lau A, So RWL, Lau HHC, Sang JC, Ruiz-Riquelme A, Fleck SC et al. (2020) α-Synuclein strains target distinct brain regions and cell types. Nat Neurosci 23:21–31. 10.1038/s41593-019-0541-x [PubMed: 31792467]
29. Lavenir I, Passarella D, Masuda-Suzukake M, Curry A, Holton JL, Ghetti B et al. (2019) Silver staining (Campbell-Switzer) of neuronal α-synuclein assemblies induced by multiple system atrophy and Parkinson's disease brain extracts in transgenic mice. Acta Neuropathol Commun 7:148. 10.1186/s40478-019-0804-5 [PubMed: 31522685]
30. Li B, Ge P, Murray KA, Sheth P, Zhang M, Nair G et al. (2018) Cryo-EM of full-length α-synuclein reveals fibril polymorphs with a common structural kernel. Nat Commun 9:3609. 10.1038/s41467-018-05971-2 [PubMed: 30190461]
31. Luk KC, Kehm V, Carroll J, Zhang B, O'Brien P, Trojanowski JQ et al. (2012) Pathological α-synuclein transmission initiates Parkinson-like neurodegeneration in nontransgenic mice. Science 338:949–953. 10.1126/science.1227157 [PubMed: 23161999]
32. McKeith IG, Boeve BF, Dickson DW, Halliday G, Taylor JP, Weintraub D et al. (2017) Diagnosis and management of dementia with Lewy bodies: fourth consensus report of the DLB consortium. Neurology 89:88–100. 10.1212/wnl.0000000000004058 [PubMed: 28592453]
33. McKeith IG, Dickson DW, Lowe J, Emre M, O'Brien JT, Feldman H et al. (2005) Diagnosis and management of dementia with Lewy bodies: third report of the DLB consortium. Neurology 65:1863–1872. 10.1212/01.wnl.0000187889.17253.b1 [PubMed: 16237129]
34. McLean CA, Cherny RA, Fraser FW, Fuller SJ, Smith MJ, Beyreuther K et al. (1999) Soluble pool of Abeta amyloid as a determinant of severity of neurodegeneration in Alzheimer's disease. Ann Neurol 46:860–866. 10.1002/1531-8249(199912)46:6<860::aid-ana8>3.0.co;2-m [PubMed: 10589538]
35. Nelson PT, Jicha GA, Kryscio RJ, Abner EL, Schmitt FA, Cooper G et al. (2010) Low sensitivity in clinical diagnoses of dementia with Lewy bodies. J Neurol 257:359–366. 10.1007/s00415-009-5324-y [PubMed: 19795154]
36. Nizynski B, Dzwolak W, Nieznanski K (2017) Amyloidogenesis of Tau protein. Protein Sci 26:2126–2150. 10.1002/pro.3275 [PubMed: 28833749]
37. Peng C, Gathagan RJ, Covell DJ, Medellin C, Stieber A, Robinson JL et al. (2018) Cellular milieu imparts distinct pathological α-synuclein strains in α-synucleinopathies. Nature 557:558–563. 10.1038/s41586-018-0104-4 [PubMed: 29743672]
38. Peng Z, Parker AS, Peralta MDR, Ravikumar KM, Cox DL, Toney MD (2017) High tensile strength of engineered β-solenoid fibrils via sonication and pulling. Biophys J 113:1945–1955. 10.1016/j.bpj.2017.09.003 [PubMed: 29117519]
39. Polinski NK, Volpicelli-Daley LA, Sortwell CE, Luk KC, Cremades N, Gottler LM et al. (2018) Best practices for generating and using alpha-synuclein pre-formed fibrils to model Parkinson's disease in rodents. J Parkinsons Dis 8:303–322. 10.3233/jpd-171248 [PubMed: 29400668]

40. Prusiner SB, Woerman AL, Mordes DA, Watts JC, Rampersaud R, Berry DB et al. (2015) Evidence for α-synuclein prions causing multiple system atrophy in humans with parkinsonism. Proc Natl Acad Sci USA 112:E5308–5317. 10.1073/pnas.1514475112 [PubMed: 26324905]
41. Rossi M, Candelise N, Baiardi S, Capellari S, Giannini G, Orrù CD et al. (2020) Ultrasensitive RT-QuIC assay with high sensitivity and specificity for Lewy body-associated synucleinopathies. Acta Neuropathol 140:49–62. 10.1007/s00401-020-02160-8 [PubMed: 32342188]
42. Ruf VC, Shi S, Schmidt F, Weckbecker D, Nübling GS, Ködel U et al. (2020) Potential sources of interference with the highly sensitive detection and quantification of alpha-synuclein seeds by qRT-QuIC. FEBS Open Bio 10:883–893. 10.1002/2211-5463.12844
43. Sanderson JB, De S, Jiang H, Rovere M, Jin M, Zaccagnini L et al. (2020) Analysis of α-synuclein species enriched from cerebral cortex of humans with sporadic dementia with Lewy bodies. Brain Commun 2:fcaa010. 10.1093/braincomms/fcaa010 [PubMed: 32280944]
44. Schweighauser M, Shi Y, Tarutani A, Kametani F, Murzin AG, Ghetti B et al. (2020) Structures of α-synuclein filaments from multiple system atrophy. Nature 585:464–469. 10.1038/s41586-020-2317-6 [PubMed: 32461689]
45. Shahnawaz M, Mukherjee A, Pritzkow S, Mendez N, Rabadia P, Liu X et al. (2020) Discriminating α-synuclein strains in Parkinson's disease and multiple system atrophy. Nature 578:273–277. 10.1038/s41586-020-1984-7 [PubMed: 32025029]
46. Smith JF, Knowles TP, Dobson CM, Macphee CE, Welland ME (2006) Characterization of the nanoscale properties of individual amyloid fibrils. Proc Natl Acad Sci USA 103:15806–15811. 10.1073/pnas.0604035103 [PubMed: 17038504]
47. Strohäker T, Jung BC, Liou SH, Fernandez CO, Riedel D, Becker S et al. (2019) Structural heterogeneity of α-synuclein fibrils amplified from patient brain extracts. Nat Commun 10:5535. 10.1038/s41467-019-13564-w [PubMed: 31797870]
48. Tarutani A, Arai T, Murayama S, Hisanaga SI, Hasegawa M (2018) Potent prion-like behaviors of pathogenic α-synuclein and evaluation of inactivation methods. Acta Neuropathol Commun 6:29. 10.1186/s40478-018-0532-2 [PubMed: 29669601]
49. Van der Perren A, Gelders G, Fenyi A, Bousset L, Brito F, Peelaerts W et al. (2020) The structural differences between patient-derived α-synuclein strains dictate characteristics of Parkinson's disease, multiple system atrophy and dementia with Lewy bodies. Acta Neuropathol 139:977–1000. 10.1007/s00401-020-02157-3 [PubMed: 32356200]
50. van Steenoven I, Majbour NK, Vaikath NN, Berendse HW, van der Flier WM, van de Berg WDJ et al. (2018) α-Synuclein species as potential cerebrospinal fluid biomarkers for dementia with lewy bodies. Mov Disord 33:1724–1733. 10.1002/mds.111 [PubMed: 30440090]
51. Waters CH, Miller CA (1994) Autosomal dominant Lewy body parkinsonism in a four-generation family. Ann Neurol 35:59–64. 10.1002/ana.410350110 [PubMed: 8285594]
52. Xue WF, Hellewell AL, Gosal WS, Homans SW, Hewitt EW, Radford SE (2009) Fibril fragmentation enhances amyloid cytotoxicity. J Biol Chem 284:34272–34282. 10.1074/jbc.M109.049809 [PubMed: 19808677]

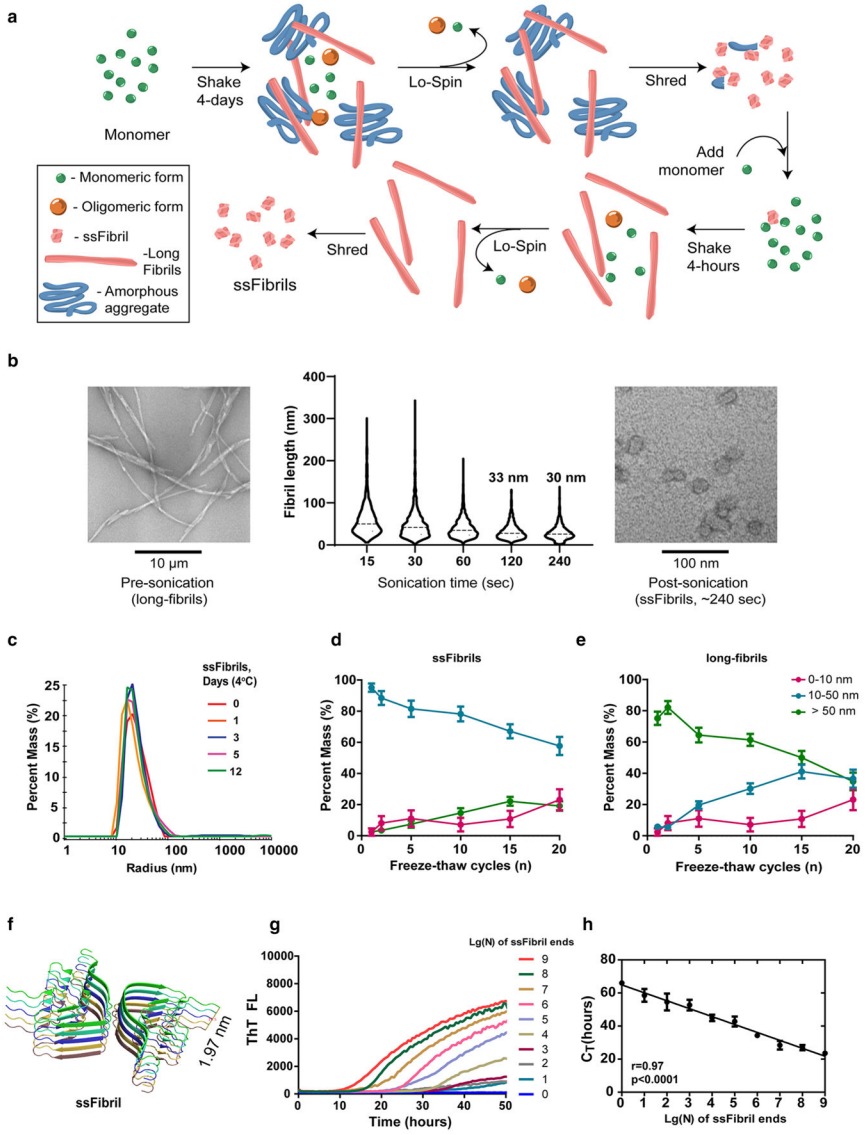

Fig. 1.

Single-molecule quantification of temperature and time-stable ssFibrils with quantitative RT-QuIC (qRT-QuIC). **a** Schematic for the purification of short-stumpy α-synuclein fibrils (ssFibrils). A long initial shaking round in saline (pH 7.4) results in an admixture of long α-synuclein rod fibrils, amorphous aggregates, oligomers, and unpolymerized monomer. Heavy insoluble fibrils and aggregates are separated from unpolymerized proteins and small oligomers through brief low-speed centrifugation. Pelleted heavy particles are then subjected to strong-sonication (otherwise known as shredding). The shredded aggregates are diluted (0.1% w/v) into a secondary rapid fibril elongation reaction. Isolation, washing, and sonication of these heavy fibril products results in the generation of enriched short-stumpy fibrils, or ssFibrils. **b** Representative transmission electron microscopy images and analysis of ($n > 1000$ particles measured over three experiments) human α-synuclein full-length fibrils, and processed ssFibrils. **c** Dynamic light-scattering size distributions of ssFibrils after extended incubations in saline buffer at 4 °C. **d** Light-scattering measures of ssFibrils after

extensive repetitive freeze thaw cycles. **e** Light-scattering measures of long α-synuclein rod fibrils subjected to the same repetitive freeze thaw cycling. **f** Rendered stack representations of α-synuclein monomers (n = 10 monomers shown) from rod fibrils formed from spontaneous α-synuclein fibrillization, as described [30]. **g** Representative real-time quaking-induced conversion shown as decadic logarithmic performance over known quantities of ssFibrils. Calculated fibril-forming units (FFUs) are indicated, with the assumption of two-fibril-forming ends/particle. Lg(0) indicates reactions with no ssFibrils added, indicating spontaneous fibrillization. **h** Optimal log-linear regression analysis based on calculated C_T values from triplicate reactions (see Supplemental Fig. 2). Error bars represent SEM, dots indicate mean group values from at least three independent experiments, and each Lg(N) curve shown represents the calculated average of at least three independent experiments

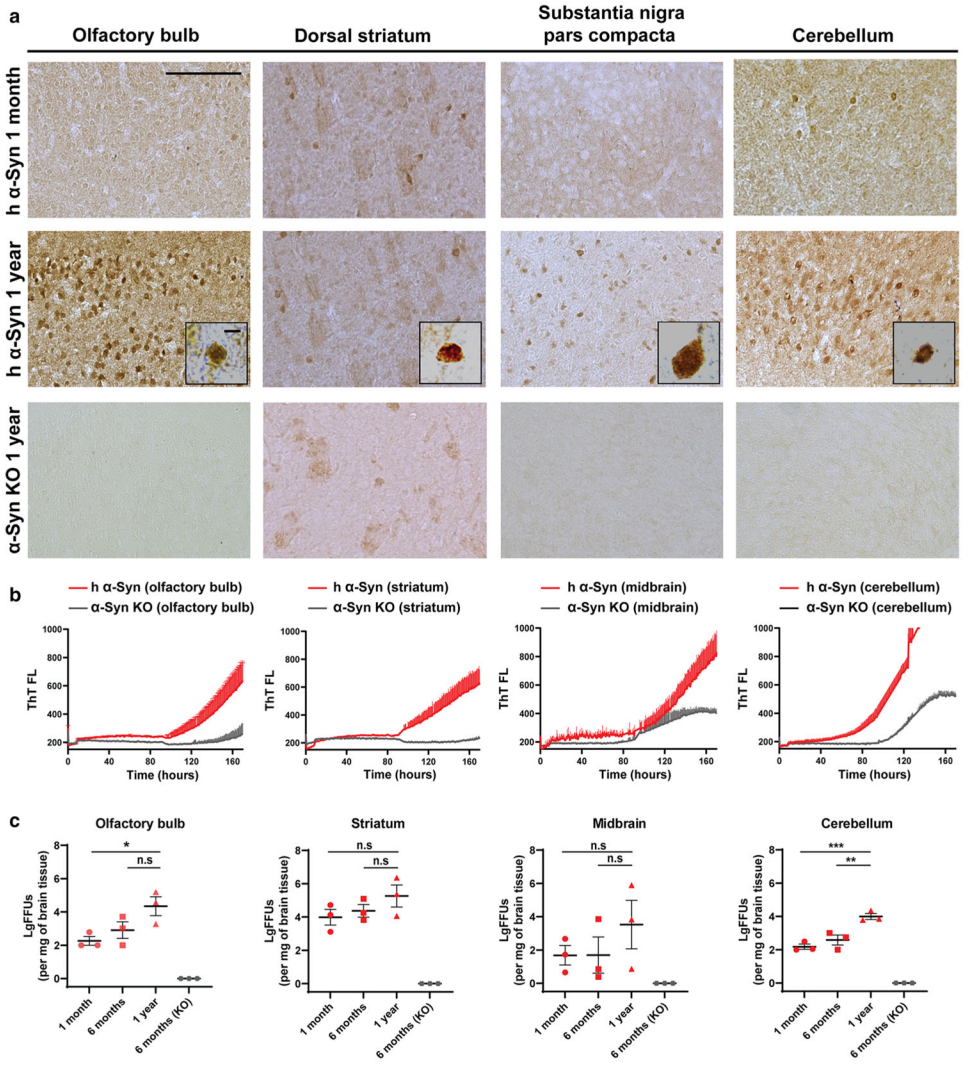

Fig. 2.

Early soluble fibril-forming activity in humanized WT-α-synuclein mouse brain that precedes pS129-α-synuclein deposition. **a** Representative immunostained coronal brain sections of phospho-α-synuclein (pS129, depicted with brown coloration) in the olfactory bulb, dorsal striatum, substantia nigra pars compacta, or cerebellum, of 1 month-old, or 1 year-old, mice that express only human α-synuclein, ~ fourfold (whole-brain) over the levels of α-synuclein in non-transgenic mice (Supplemental Fig. 3). pS129-α-synuclein staining conditions were selected based on a lack of signal under the same processing conditions in α-synuclein knock-out (KO) animals, and as previously described [13]. High magnification insets show typical perinuclear accumulations of pS129-α-synuclein reactivity. Scale bars show 0.5 mM and 5 μM in the insets. **b** Representative human α-synuclein permissive templating activity in qRT-QuIC reactions from brain extracts of olfactory bulb, striatum, midbrain, and cerebellum, from 1-year-old humanized α-synuclein mice or α-synuclein KO mice. Each curve shown represents the average of three qRT-QuIC reactions from three mice performed in triplicate. Males and female mice are equally represented. **c** LgFFUs per mg of brain tissue were calculated from triton X-100-solubilized fractions of freshly procured

tissue from the olfactory bulb, striatum, midbrain and cerebellum of 1-year, 6-month and 1 month-old WT-hPAC-α-synuclein/m-α-synuclein KO mice. Each group column represents mean values from the analysis of $n = 3$ mice/group, with each data point indicating the mean calculated FFU value extrapolated from C_T values derived from reference standards of ssFibrils spiked into corresponding triton-solubilized homogenates from α-synuclein KO mice. Analysis was performed with one-way ANOVA and Holm–Sidak's multiple comparison test, 1 year-old values compared to the indicated groups, where n.s. is not significant, $*p < 0.05$, $**p < 0.01$, $***p < 0.001$

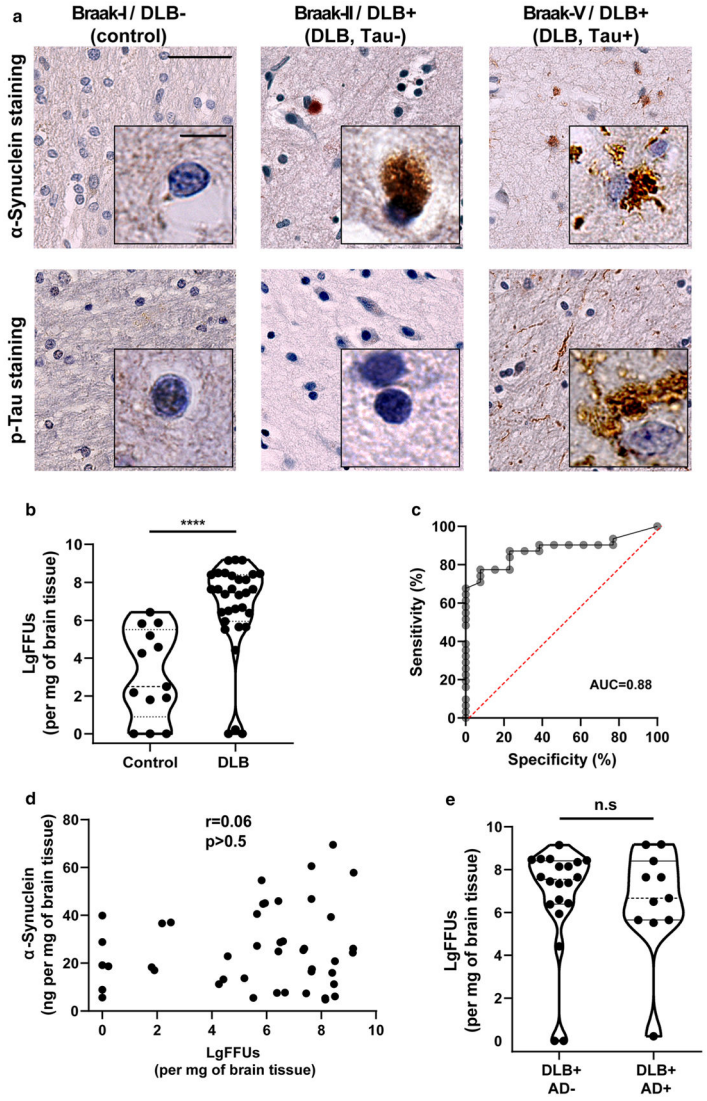

Fig. 3.

qRT-QuIC analysis of neocortical tissue from DLB, with or without concomitant AD pathology. **a** Representative immunostained neocortical brain sections for α-synuclein or phospho-tau (AT8) from neuropathologically normal controls (AD−/PD−/DLB−), or cases with a diagnosis of DLB (neocortical-dominant subtype), without AD pathology, or with concomitant neocortical tau and amyloid (tau + [Braak IV–VI]/DLB+,). **b** Quantification of log-fibril-forming units (LgFFUs) per mg of brain tissue measured in triton X-100 solubilized neocortical brain homogenates from frozen tissue of subjects diagnosed with neocortical-dominant DLB and normal controls, with spike-in standards of reference ssFibrils spiked into human brain control homogenates negative for detectable FFUs. **c** Receiver operating curves (ROC) for group discrimination between DLB (all subjects, Extended Table 1) and controls, with percent of sensitivity and specificity for LgFFUs (per mg of brain tissue) at 87 and 77, respectively. **d** Correlation analysis of α-synuclein concentration and LgFFUs per mg of brain tissue. Spearman coefficients and corresponding *p* values are indicated. **e** Violin plots representing distributions of LgFFUs per mg of brain

tissue relative to AD neuropathology. Group comparison analysis for panel b and e uses two-way unpaired *t* tests, where n.s. is not significant and ****$p < 0.0001$. Each data point represents the mean value calculated from at least three independent experiments (i.e., qRT-QuiC runs)

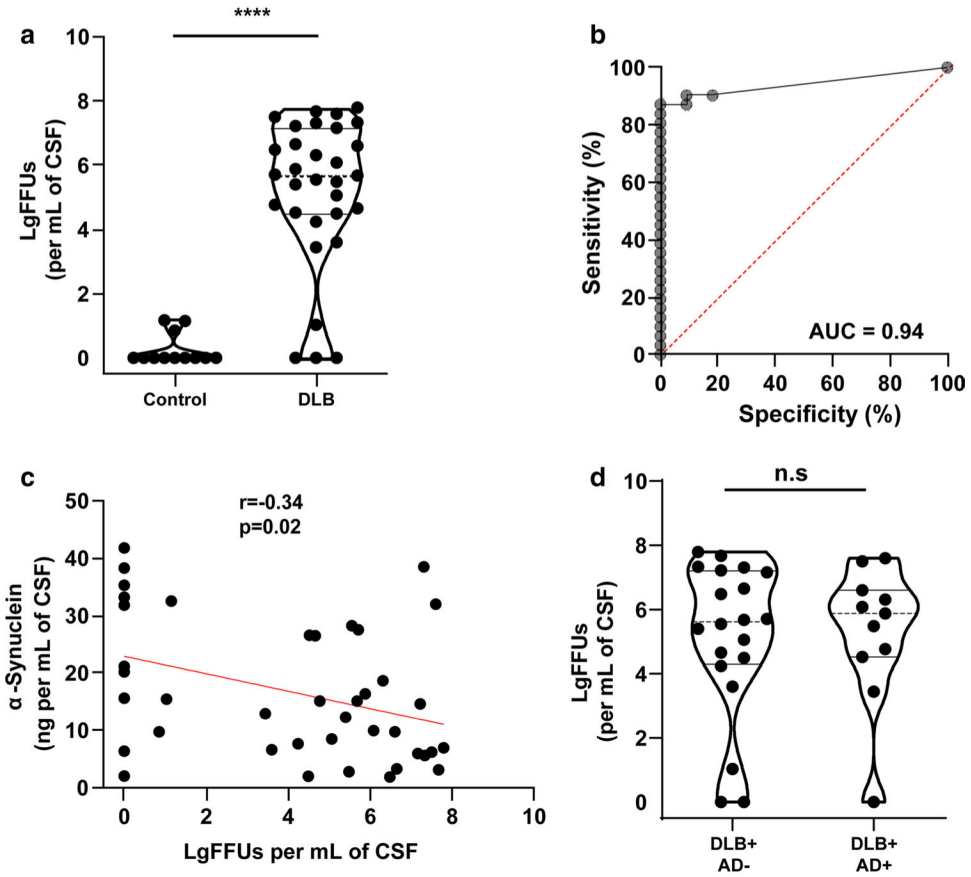

Fig. 4.

qRT-QuIC analysis of CSF from DLB. **a** Quantification of fibril-forming units (FFUs) per mL in brain-matched CSF from subjects with a pathological diagnosis of neocortical DLB (Table 1) and normal controls, with spike-in standards of ssFibrils into CSF that was previously identified as negative for fibril activity. **b** ROC group discrimination for assessing qRT-QuIC accuracy in resolving a pathological diagnosis of DLB from controls. Percent sensitivity and specificity are 87 and 100. **c** Correlation analysis of total α-synuclein concentration and LgFFUs per mL in CSF. Spearman coefficients and corresponding p values are indicated. **d** Violin plots representing distributions of LgFFUs (calculated per mL of CSF) to AD neuropathology. Spearman coefficients and corresponding p values are indicated. Comparison analysis for panel a and d uses a two-tailed unpaired t test, where n.s. is not significant and **** $p < 0.0001$. Each data point represents the mean value calculated from at least three independent experiments

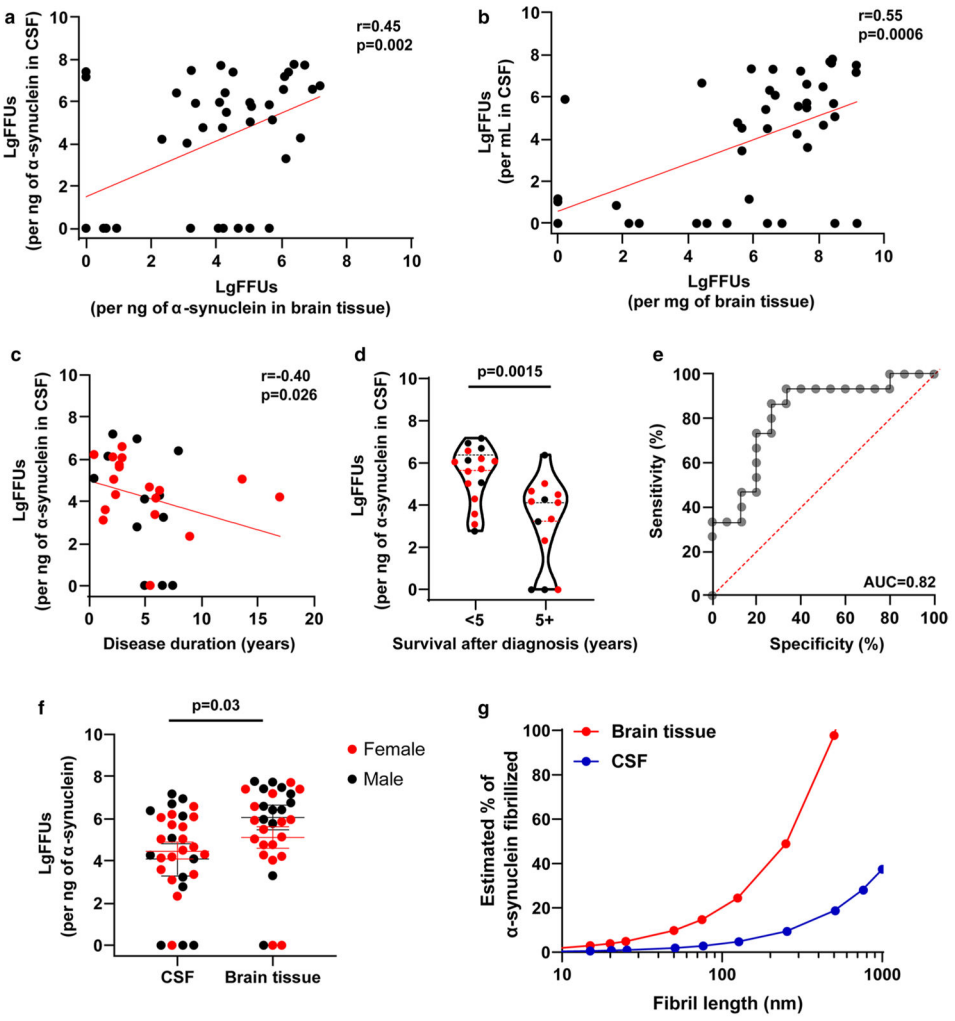

Fig. 5.

High concentrations of fibril activity in CSF correlates with reduced survival. **a** Correlation in log-fibril-forming units (LgFFUs) between CSF and brain tissue, normalized to nanograms of α-synuclein or **b** per mL of CSF and per mg of brain tissue. **c** Scatter plot between LgFFUs found in CSF and years of survival after a diagnosis of dementia, with sex separated by color (male = black, female = red). **d** Group analysis of study subjects with early mortality (< 5 years) or later mortality (> 5 years) after a diagnosis of dementia, with sex separated by color (male = black, female = red). **e** ROC assessment for survival in DLB with the area-under the curve (AUC) shown corresponding to a sensitivity of 87 and specificity at 73. **f** Comparison of LgFFUs per ng of α-synuclein in CSF and per ng of α-synuclein in brain tissue, with sex separated by color (male = black, female = red). All correlation values are spearman coefficients with corresponding p values. Group comparison analyses include two-tailed unpaired t tests for total number of cases, as well as ordinary two-way ANOVA with Sidak's multiple comparison test for the evaluation of sex as a covariable (see "Results" section). Each data point represents the mean value calculated from at least three independent experiments. **g** Hypothetical relationship between the average size of fibrils to the minimum percent of α-synuclein constrained into template-

permissive fibrils. Estimates are based on the observed (mean) amount of total α-synuclein found in brain tissue or CSF in this study. Thus, each data point represents an average number of FFUs at any given average length of fibril, assuming a normal distribution of fibril lengths in solution

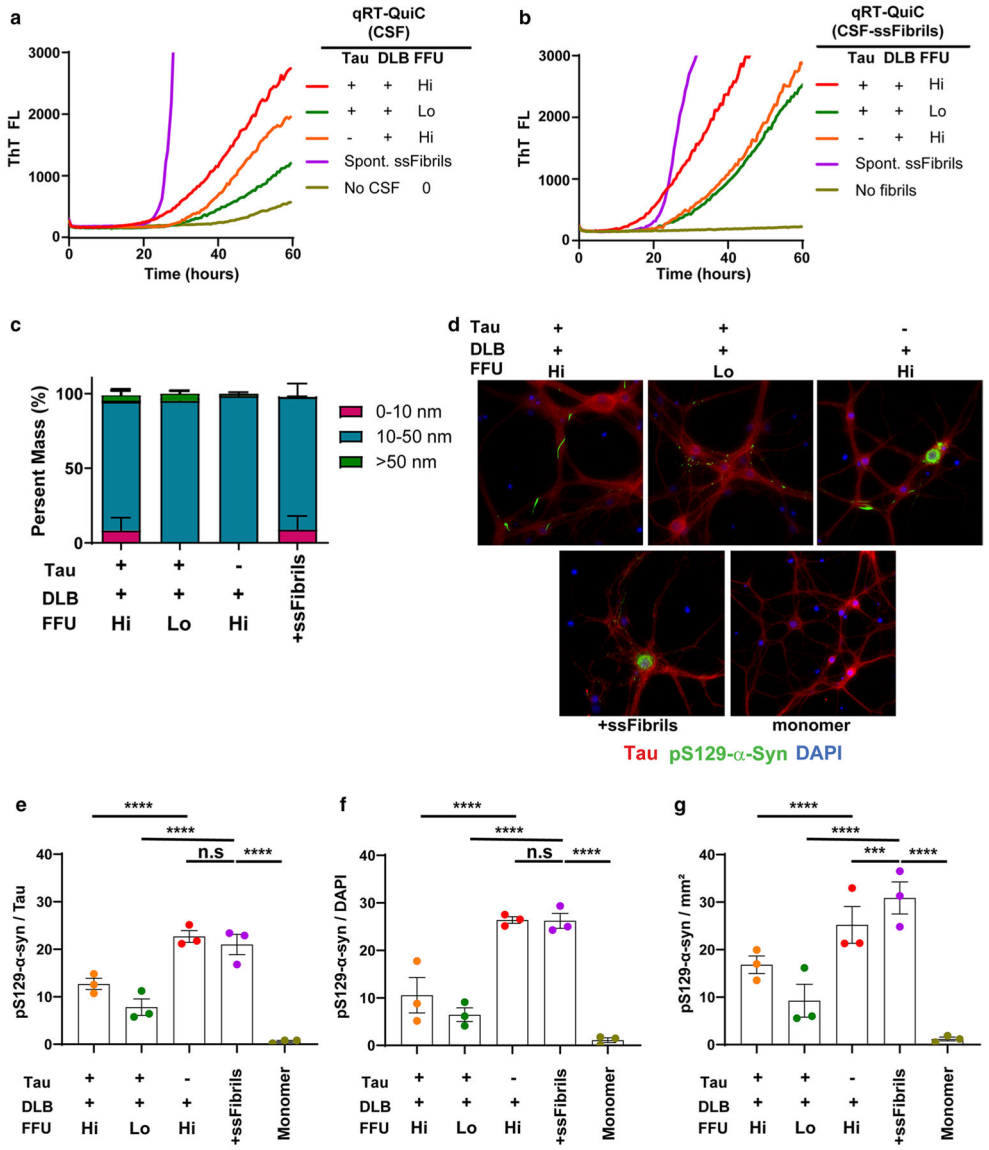

Fig. 6.

Seeding characteristics of DLB-amplified strains. **a** Representative quantitative (qRT-QuIC) analysis of three CSF samples from DLB cases categorized (as in Fig. 4) with the highest concentrations of FFUs (Hi, LgFFUs > 6/mL), or lower concentrations (Lo, LgFFUs < 4/mL). Samples pathologically evaluated as Braak stage > 3 are marked as Tau "+"; samples with Braak stage < 3 shown are marked as Tau "−". Also shown are representative results from a spike-in concentration (6.5 pM) of spontaneously generated ssFibrils (labeled "Spont. ssFibrils"). **b** Equivalent concentrations (6.5 pM) of ssFibrils purified from reaction products from panel a, derivative from plateaued (thioflavin-T) reactions, were added into a second qRT-QuIC reaction for fibril elongation templating. Representative thioflavin-T fluorescence curves with or without (labeled "No fibrils") added into reactions are given. **c** Representative fluorescent images of pS129-α-synuclein staining in primary hippocampal neuronal cultures cultured from humanized α-synuclein mice, 10-days (DIV17) after ssFibril addition. **d** 0.65

nM ssFibrils particles or monomer control, 70 nM, were added at DIV7. Red color indicates tau staining, green color indicates pS129-α-synuclein staining, and blue color indicates DAPI. **e** Group analysis of pS129-α-synuclein occupancy normalized to percent of tau occupancy in images, or **f** pS129-α-synuclein occupancy normalized to the number of distinct DAPI spots (i.e., nuclei), or **g** pS129-α-synuclein occupancy normalized to mM^2 area of the culture wells. Every data point represents the mean of signal curated from an individual litter (two well replicates for each litter) of humanized α-synuclein mice. Raw data for each image processed is presented in Supplemental Fig. 8. Significance is assessed by ordinary two-way ANOVA with Dunnett's multiple comparison post-hoc test (all groups compared to ssFibrils), and p values are indicated in panels f, g and h, where n.s. is not significant, ***$p < 0.001$, ****$p < 0.0001$

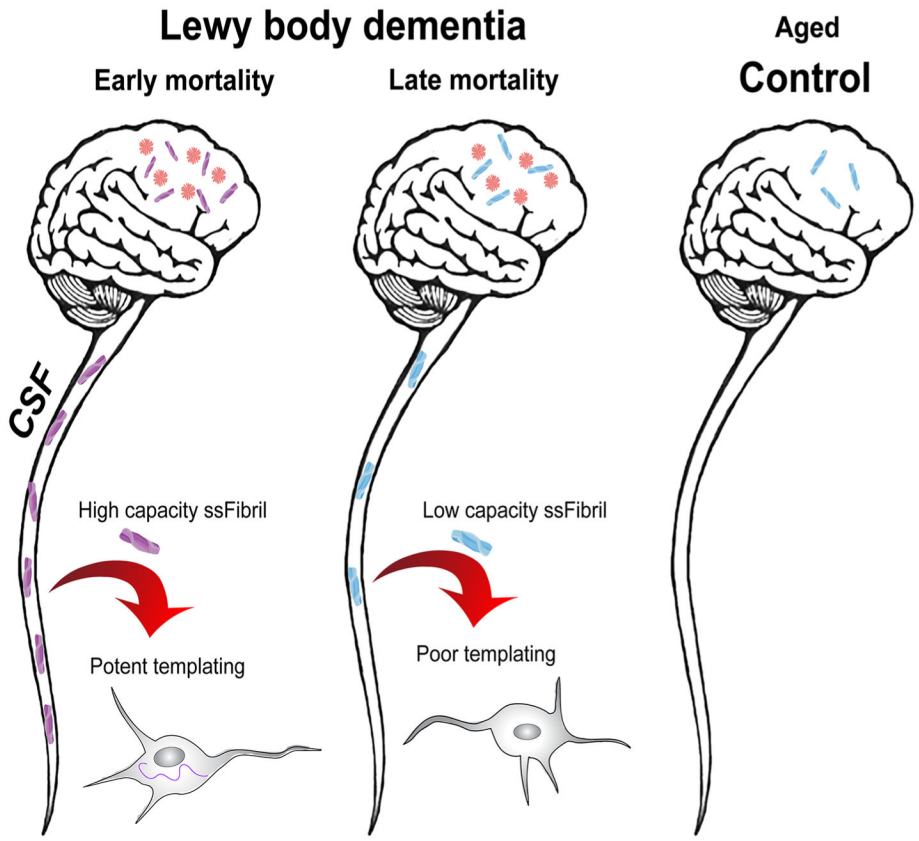

Fig. 7.

Model for α-synuclein fibril heterogeneity associated with survival in Lewy body dementia. Fibril activity is highest in DLB cerebrospinal fluid in cases with low survival rates subsequent to a diagnosis of dementia. Specific levels of neocortical fibril activities in the brain spill over to activities in CSF. However, in controls without disease, low fibril activity was detected in brain tissue but not in CSF. This model implies that the presence of fibrils alone in brain tissue, without ongoing disease processes (e.g., neurodegeneration), is not enough to release fibrils through to CSF. Equimolar application of α-synuclein amplified strains to neurons demonstrates potent templating activity in fibrils amplified from the CSF of individuals with high fibril activity (and low survival in disease) compared to poor templating activity in fibrils amplified from individuals with low fibril activity

Table 1

DLB case and control cohort characteristics

	DLB	Control
N, total (*N*, females)	31 (18)	14 (5)
Age, years, mean (± SD)	76 (6)	85 (5)
Braak stage, mean (± SD)	4 (1)	2 (1)
CERAD, mean (± SD)	2 (1)	0 (1)
TAP, mean (± SD)	4 (1)	1 (1)
Disease duration, years[a], mean (± SD)	5.15 (3.5)	NA
AD pathology, *N* (*N*, females)	11 (6)	0 (0)
MMSE[b], mean(± SD)	16 (11)	28 (6)
Post-mortem interval, h, mean (± SD)	13.07 (9.3)	15 (8.5)

Braak stage Braak stages of tau pathology, *CERAD* consortium to establish a registry for Alzheimer's disease, *TAP* ThaI Aβ phase, *MMSE* mini-mental state examination

[a]Time (years) from dementia diagnosis to death

[b]Available for only ten DLB cases and only 13 controls